

Genes within Bottles. Synergism Between Simulation and Experiment in Designing Nanovectors for DNA/RNA Delivery

D. Marson,^a V. Dal Col,^a P. Posocco,^a E. Laurini,^a M. Fermeglia,^a and S. Pricl^{a,b,*}

^aMolecular Simulation Engineering (MOSE) Laboratory,
Department of Industrial Engineering and Information Technology (DI3),
via Valerio 10, 34127 Trieste, Italy

^bNational Interuniversity Consortium for Material Science
and Technology (INSTM), Research Unit MOSE-DI3,
University of Trieste

Original scientific paper
Received: May 4, 2012
Accepted: July 26, 2012

Due to their relative easy synthesis and commercial availability, nanovectors based on dendrimers and dendrons are among the most utilized non-viral vectors for gene transfer. Concomitantly, recent advances in molecular simulations and computer architectures not only allow for accurate predictions of many structural, energetical, and eventual self-assembly features of these nanocarriers *per se*, but are able to yield fundamental information about the interactions of these nanovectors with their nucleic acid cargoes at a molecular level. In this work, we aim at reviewing some of our own efforts in the field of multiscale molecular modeling of these fascinating materials. This review is written by computational scientists for experimental scientists, with the specific purpose of illustrating the potentiality of these methodologies and the usefulness of multiscale molecular modeling as an innovative and complementary tool in their current research.

Key words:

Multiscale molecular modeling; dendrimers; dendrons; self-assembly; gene therapy.

Nanotechnology and drug delivery

The predominant methods to deliver drugs are oral and injection, which has limited the progress of drug development. Most drugs have been formulated to accommodate *per os* or intramuscular/intravenous delivery routes, which are not always the most efficient means for a particular therapy. New biologic drugs such as proteins and nucleic acids (NAs) require novel delivery technologies that will minimize side effects and lead to better patient compliance. Market forces are also driving the need for new, effective drug delivery methods; meanwhile, patent expirations are driving pharmaceutical companies to reformulate their products. Furthermore, drug candidates that did not pass through the trials phases may be reformulated to be used with new drug delivery systems.

Innovative drug delivery systems may make it possible to use certain chemical entities or biologics that were previously impractical because of their toxicity or because they were impossible to administer. For example, drug targeting is enabling the delivery of chemotherapeutic agents directly to tumors, thereby drastically reducing systemic side effects. The current research in the field is continu-

ally pursuing new ways to deliver macromolecules that will facilitate the development of new biological products such as bio-blood proteins and bio-vaccines. Similarly, the success of DNA- and RNA-based therapies will dramatically depend on the availability of effective drug delivery techniques.

In addition to the commonly used oral and injection routes, drugs can also be administered through other means, including transdermal, transmucosal, ocular, pulmonary, and implantation. The mechanisms used to achieve alternative drug delivery typically incorporate one or more of the following materials: biologics, polymers, silicon-based materials, carbon-based materials, or metals. The substances are structured in microscale and, more recently, nanoscale formats.

The United States National Nanotechnology Initiative (NNI), launched in October 2000, has formulated ten potential research and development targets to be reached by 2015. Five of these research goals are relevant to drug development and delivery: i) no suffering and death from cancer when treated, ii) advanced materials and manufacturing, iii) pharmaceutical synthesis and delivery, iv) converging technologies from the nanoscale, and v) life-cycle biocompatible/sustainable development. This emphasis exemplifies the importance of nanotechnology in the progress of medicine.

*Corresponding author: phone: +39-040-5583750. fax: +39-040-569823.
E-mail: Sabrina.Pricl@di3.units.it

Generally speaking, the efficiency of drug delivery to various part of the body is directly affected by particle size. Nanostructure-mediated drug delivery, a key technology for the realization of nanomedicine, has the potential to enhance drug bioavailability, improve the timed release of drug molecules, and enable precision drug targeting. Nanoscale drug delivery systems can be implemented within pulmonary therapies, as gene delivery vectors, and in stabilization of molecules that would otherwise degrade too rapidly. Additional benefits of using targeted nanoscale drug carriers are reduced drug toxicity and more efficient drug distribution. Anatomic features such as the blood-brain barrier, the branching pathway of the lungs, and the tight epithelial junctions of the skin make it difficult for drugs to reach the desired pathological targets. Nanostructured drug carriers may substantially help to penetrate or overcome these hurdles to drug delivery. Advantages of nanostructure-mediated drug delivery further include the ability to deliver drug molecules directly into cells, and the capacity to target tumors within healthy tissues:^{2h)} in fact, nanoscale drug delivery architectures are able to penetrate tumors due to the discontinuous (or *leaky*) nature of the tumor microvasculature, which typically contains pores ranging from 100 to 1000 nm in diameter (see below). The microvasculature of healthy tissues varies by tissue type, but in most tissues including the heart, brain, and lung, there are tight intercellular junctions less than 10 nm wide. Therefore, tumor within these tissue types can be selectively targeted by creating drug delivery nanostructures greater than the intercellular gap of the healthy tissue but smaller than the pores found within the tumor vasculature.

Equally important, through the precise control of the drug carrier architecture, the release profile of the drug can be tuned to achieve a desired kinetic profile. As a common notion, the ideal release profile for most conventional drugs would follow a steady release rate so that the drug levels in the body remains constant while the drug is being administered.

So far, various nanoscale architectures can be realized to achieve efficient drug transport and near zero-order release kinetics, and these include solid and hollow nanospheres, nanotubes, and linear/branched/hyperbranched macromolecules. To generate the required nanostructures, different fabrication methods can be used depending on the specific type and nature of the materials, comprising molecular self-assembly, bio-aggregation, nanomanipulation, photochemical patterning, molecular imprinting, layer-by-layer electrostatic or vapor deposition.

Gene delivery: a primer

With the conclusion of the human genome-sequencing project, the medical research community has an unparalleled opportunity to understand and cure diseases on a genetic level. Specifically, gene therapy aims at delivering DNA, RNA, or antisense sequences that alter gene expression within a specific cell population, thereby manipulating cellular processes and responses. A naked DNA/RNA injection into local tissues or into the systemic circulation is probably the simplest and safest approach to gene therapy. However, due to the rapid degradation by nucleases and fast clearance by the mononuclear phagocyte system, the gene expression/silencing level and the area of tissue treated after a bare nucleic acid injection are severely limited. Consequently, the development of gene therapy vectors with sufficient targeting ability, transfection efficiency, and safety must be achieved before gene therapy can be routinely used in man. Perhaps, foremost among these is the issue of delivery. The *in vivo* use of DNA/small-interfering RNA (siRNA) effective against cancer or other genetic diseases relies on the availability of a delivery vehicle that can be systematically administered to reach the target cells. Moreover, because sufficient intact, functional genetic material must be delivered into cells to reach an effective intracellular concentration, and to limit potential side effects due to a randomized, general transfection of normal, non-target tissues, it is also crucial to develop means of directing such a delivery vehicle specifically to the target cells.⁵

Synthetic nanoscale drug delivery systems, or *nanovectors*, offer exciting perspectives in this respect. They can be structurally varied, are relatively safe to produce, and are able to carry large and diverse genetic material into cells. Accordingly, studying their biological and physico-chemical properties by structural modification represents an exciting challenge for chemists as this approach constantly provides new and valuable information for the design of more complex and efficient systems.^{2c), 2f)} However, any synthetic agent to deliver genetic material specifically will be exposed to biological mechanisms that unavoidably limit its trafficking both outside and inside the cells, as exemplified in Figure 1.

In summary, an ideal nanovector should tightly compact the foreign nucleic acid, transport it through cellular membranes while ensuring its protection from degradation and allow its recognition and activation by the cell machinery. Of course, the synthesis of a *magic bullet* affording all these skills together remains idealistic; nevertheless, many synthetic vectors have been active enough to justify

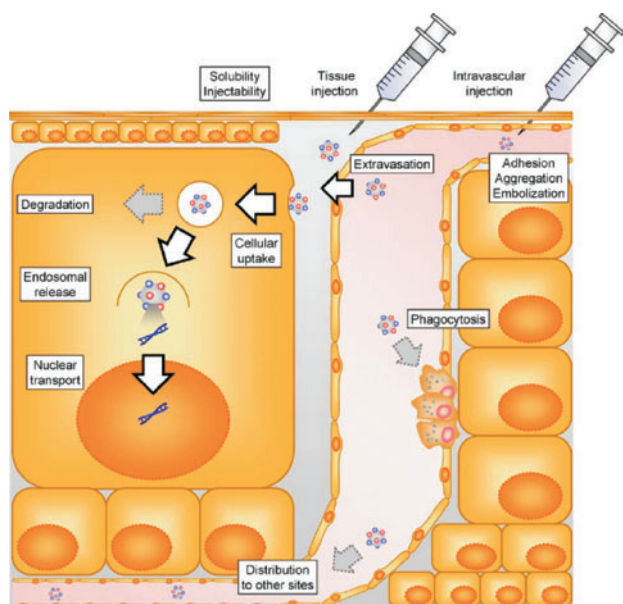


Fig. 1 – Hurdles in gene delivery following in vivo administration. The (nano)vector system should be soluble and injectable, avoid adhesion (i.e., non-specific binding) to tissues, aggregation, embolization, and phagocytosis, extravasate, find a way to the inside of the target cells, escape from the endosomal/lisosomal degradation and, in some cases, be transported into the nucleus. Reprinted with permission from Nishikawa, M.; Takakura, Y.; Hashida, M. Theoretical considerations involving the pharmacokinetics of plasmid DNA. *Adv. Drug Delivery Rev.*, 2005, 57, 675–688. Copyright {2005} Elsevier B.V.

concentrated research efforts and sometimes, even commercialization.

Dendritic nanovectors for gene therapy

Dendrimers and dendrons are classes of macromolecules with highly branched three-dimensional architectures whose structural elements can be tuned to affect both surface and internal properties of the macromolecules themselves. Dendrimer structures can be divided into three main components: a core, an interior, and a shell (see Figure 2a). The *core* affects the overall 3D shape of the molecule (spherical, ellipsoidal, cylindrical, etc.), the *interior* influences the eventual capacity of the macromolecule to host small-molecule guests and, finally, the *outer* shell can be functionalized to maximize the interactions with a cargo agent and/or with, e.g., a given receptor on the cell surface. The number of branch points increases upon moving from the dendrimer core to its surface and defines the so-called dendrimer *generation* (*G*). Dendrons (Figure 2b) are wedge-shaped dendrimer sections with multiple terminal groups and a single reactive function at the focal point. In addition to the dendrimer features described above, dendrons offer the extra-option of orthogonal reactions utilizing the distinct focal point.

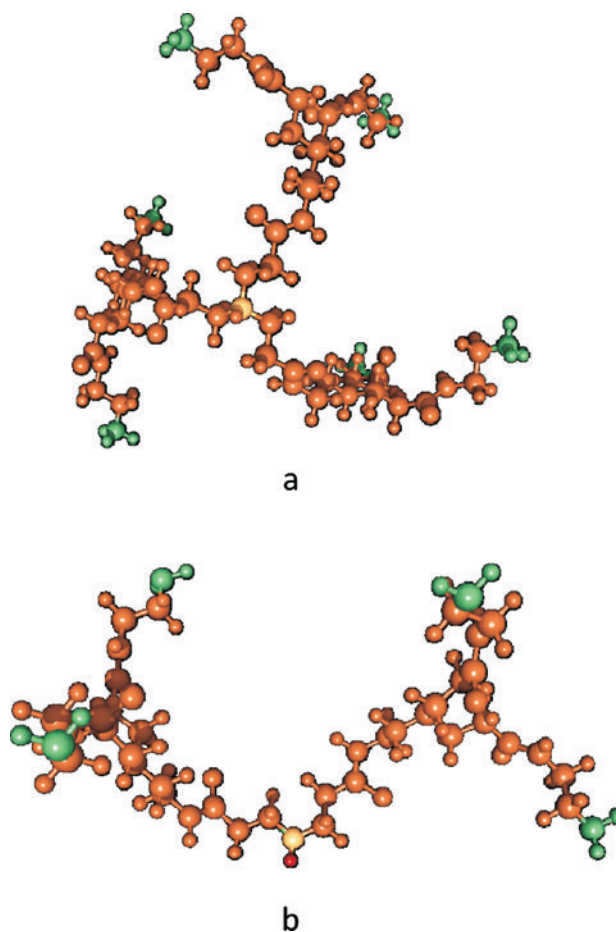


Fig. 2 – (a) Model structure of a generation 2 (*G*₂) dendrimer featuring ammonia as the core and amidoamine as the repeating (branching) units. The ammonia core nitrogen atom is in a sandy brown color, the dendrimer interior (branches) are painted in sienna, while the terminal $-NH_2$ groups constituting the outer shell are colored in sea green. (b) Model structure of a *G*₂ dendron featuring ammonia as the core and amidoamine as the repeating (branching) units. The ammonia core nitrogen atom is in a sandy brown color, the dendrimer interior (branches) are painted in sienna, while the terminal $-NH_2$ groups constituting the outer shell are colored in sea green. The focal point atom amenable to further derivatization is highlighted in dark red.

Given their peculiar molecular architectures, dendrimeric nanovehicles are an attractive platform for drug delivery, in light of the presence of a central cavity and channels between their branches wherein drugs can be entrapped. In addition to drug loading within this void spaces, drug can be bound or grafted onto tailorable functional groups, as is the case of nucleic acid delivery. This affords the possibility of incorporating not only multiple and different drug molecules within the same dendrimer/dendron, but also multiple targeting ligands as well.

In aqueous conditions, dendrimer conformations are affected by ionic strength and pH, with changes depending on the type of charged groups

eventually present at the dendrimer surface. The dendrimers most widely used so far in clinical applications are the poly(amidoamine) or PAMAM dendrimers, consisting of alkyl-diamine core and tertiary amine branches. The amino surface consists of polar, highly reactive primary amine groups (Figure 2). The surfaces of the amino-functional PAMAM dendrimers are thus cationic and can be derivatized, either through ionic interactions with negatively charged molecules, or using many well-known reagents for covalent functionalization of primary amines. Importantly, at physiological pH (7.4) the primary amines are protonated in PAMAM dendrimers; this condition allows for efficient complex formation between the cationic dendritic nanovector and anionic DNA/RNA (the resulting supermolecular assembly often called *dendriplex*) mainly via electrostatic interactions.

When employed as nanovectors, dendrimers and dendrons are injected at the systemic level (intravascularly) to execute specific diagnostic and/or therapeutic missions at the biological target site. This could be a tumor mass, an inflamed portion of the vasculature, or any district within the human body where abnormal cells are proliferating. Before reaching the target site, the blood-born dendritic nanovector must make its way into the circulatory system passing a multitude of barriers that simply tend to sequester, digest and/or expel any foreign object. Additional impediments are of the biological barrier type, which include the reticular endothelial system (RES), constituted by phagocytes, specialized cells lining the liver, spleen, bone marrow, and lymphatic tissues, which recognize external molecules and remove them from the circulation. Moreover, it is important to note that the type and severity of the barrier is disease and patient specific.

However, success in targeting is not just about performance at the target site. There will be for instance loss of drug from the carrier by anticipated release or degradation, loss of the cargo/carrier complex through uptake into non-target sites, or reduced thermodynamic activity of the active principle once it is sequestered by proteins. The system may fail to reach the target in sufficient quantity, and payload release rate and the rate of diffusion of the free drug may be suboptimal to achieve therapeutic effects. It is one thing for a nanocarrier to reach a target tissue but another for its active cargo to be still bound to its vector and not lost en route or, conversely, bound too tightly that it is not released at the site of action. Recirculation of systems clearly provides further opportunity to engage with the target, but also prolongs the lifetime of the carrier in the circulation and, with most systems presently available, this increases the chances of

drug leakage and premature drug loss if release is time-dependent, rather than triggered by some mechanism (e.g., pH variation or enzymatic reaction) close to the target. Last but certainly not least, the nanovector must be devoid of any (unwanted) pharmacological action *per se*, and exert a minimum (and, if possible, null) toxic effect on both target and off-target cells.

With such a complex biological scenario, and with the multitude of possibilities chemists have at hand, devising new, efficient and safe nanovectors based only on empirical or semi-rational design has become a tantalizing task. Thus, accurate predictive mathematical or molecular models are fundamental in identifying those properties that can maximize all the structural and physico-chemical properties required to an ideal nanocarrier.

Multiscale molecular modeling for (bio)nanotechnology

In recent years, the use of computer simulations as a tool for bridging between microscopic length and time scales and the macroscopic world of the laboratory has been increasing exponentially. The main reasons for this success is that, by using computational chemistry and physics, a guess at the interactions between molecules can be provided, and 'exact' predictions of bulk properties can be obtained. The predictions are 'exact' in the sense that they can be made as accurate as we like, subject to the limitations imposed by the available computer budget. At the same time, the hidden detail behind bulk measurements can be revealed. Simulations act as a bridge in another sense: between theory and experiment. A theory can be tested by conducting a simulation using the same model. The model can be tested by comparing with experimental results. Also, simulations can be carried out on the computer that are difficult or impossible in the laboratory (for example, working at extremes of temperature or pressure).

The actual computational modeling of biological macromolecules, mainly based on molecular dynamics (MD) simulations, commonly revolves around structure representations in atomic or near-atomic detail, with a classical description of physical interactions. In a typical MD simulation, the atomic trajectories of a system of N (e.g., 10^6) particles are generated by numerical integration of Newton's equation of motion, for a specific interatomic potential, with certain initial and boundary conditions. Such models have been quite successful in complementing experimental data with structural, dynamic, and energetic information, but involve substantial computational resources for larger systems, or when long time scales have to be con-

sidered. In particular, structure-activity calculation applications, the formation and interaction of supra-molecular assemblies, and the prediction of kinetic and transport phenomena will necessarily involve extremely extensive computational resources when using models at atomic details, if they are feasible at all.

Thus, we are also in the need of developing some computational strategy to link the atomic length and time scales of MD to the macroscopic length and time scales (nanometers to micrometers and nanoseconds to microseconds): the so-called *mesoscale* phase. Only by establishing this connection from nanoscale to mesoscale it is possible to build first principles methods for describing the properties of new materials and systems for biomedical and life science applications, of which RNA/DNA delivery systems are prototypical examples.

This linking through the mesoscale in which the microstructure can be described over a length scale of tens to hundred nanometers is probably the greatest challenge to develop reliable first principles method for practical material design applications. Scale integration in specific contexts in the field of (bio)macromolecular modeling can be done in different ways. Any *recipe* for passing information from one scale to another (upper) scale is based on the proper definition of many-scale modeling which considers *objects* that are relevant at that particular scale, disregards all degrees of freedom of smaller scales, and summarizes those degrees of freedom by some representative parameters (see Figure 3).

As mentioned above, mesoscopic simulations are performed using a coarse-grained molecular model: the particle in a mesoscopic simulation is related to a group of several atoms in the corresponding atomistic simulation. Dissipative Particle Dy-

namics (DPD) is one of the best established mesoscopic simulation techniques, according to which a set of particles moves following Newton's equation of motion, and interacts dissipatively through simplified force laws. In the DPD model, individual atoms or molecules are not represented directly by the particle, but they are coarse-grained into beads (see Figure 4). These beads represent local *fluid packages* able to move independently. DPD thus offers an approach that can be used for modeling physical phenomena occurring at larger time and spatial scales than some other coarse-grained methods as it utilizes a momentum-conserving thermostat and soft repulsive interactions between the beads representing clusters of atoms/molecules.

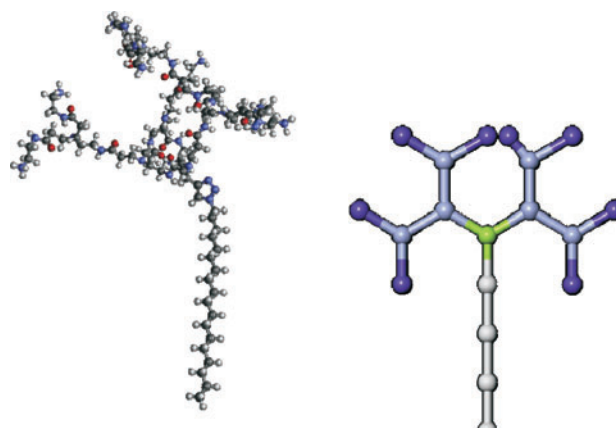


Fig. 4 – The coarse-graining concept. Atomistic (left) and coarse-grained DPD (right) representation of a modified dendron as an example.

Specifically, the multiscale modeling strategy developed by our group is based on the systematic elimination of computationally expensive degrees of freedom while retaining implicitly their influence on the remaining degrees of freedom in the mesoscopic model. At the coarse-grained (mesoscopic) level, we employed the corresponding most accurate and effective methods/simulation techniques available to investigate physical properties of each system at that level. Accordingly, using the information obtained from atomistic MD simulations we parameterized the coarse-grained (e.g., DPD) models that incorporate all essential physics/phenomena observed at the finer level. The general strategy of our multiscale modeling approach can be outlined as follows:⁶

- 1) extensive explicit solvent atomistic MD calculations on model compounds and their assembly are carried out. These simulations provide us with dynamic properties/energies that help us to identify important interactions/correlations among the nano-carriers and their cargoes which are to be used *per se*

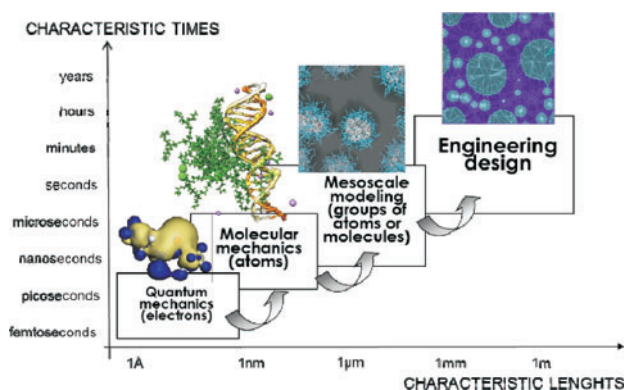


Fig. 3 – The multiscale molecular modeling concept: the information obtained from simulations at a given (lower) characteristic length and time scales is used as an input for the next (upper) scale simulations.

and/or exploited to parameterize the next scale (mesoscale) simulation models.

(2) Using conformational and structural properties obtained from MD simulations at point (1) we parameterize the DPD model in which each nanocarrier and nucleic acid segment are represented as single force centers (beads) and solvent is treated explicitly in the presence of ions and counterions. Langevin dynamics are then conducted using the DPD representation of the system. These simulations are about orders of magnitude computationally less expensive than fully atomistic simulations, therefore allowing us to simulate more realistic systems and to significantly extend the accessible time scales. Most importantly, these type of simulations yield topical information of the morphology of the systems under investigation in a length scale (L) range of $1 \leq L \leq 1000$ nm; contemporarily, the time scale can be extended up to seconds, that is, where most of the critical energetical and structural phenomena involved in several aspects of the performance of these systems take place.

(3) Eventually, the equilibrium configurations of the mesoscopic systems obtained at point (3) can be mapped back to the corresponding atomistic models, and then MD simulations can be used again to obtain more accurate structural/energetical information of the corresponding supramolecular systems (e.g., the case of self-assembled nanovectors, *vide infra*).

Under the multiscale molecular modeling perspective outlined above, the current ambitious aim of our research group is to reach the domain of nucleic acid delivery system engineering by building from fundamental principles of physics and chemistry. Hence, for fundamental predictions to play a direct role in these materials innovation and design, it is mandatory to bridge the micro-macro gap, thus establishing a tight and direct coupling between *in silico* and *in vitro/in vivo* experiments.

The importance of nanodimensions

Dendrimers (or any other macromolecule) entering the systemic circulation distribute to tissues largely via the bloodstream. Therefore, the blood flow rate determines the delivery rate of macromolecules to each tissue. Dendrimers in the circulation have direct access to the capillary endothelial cells, as well as various circulating cells in the blood. These cells have the opportunity to take up the macromolecules via specific or non-specific interactions. The interaction of macromolecules with parenchymal cells in tissues can occur only when they have access through the endothelial lining. The structure of the blood capillary walls varies greatly depending on the organ. In addition, pathological

states such as inflammation could change the structure. On the basis of the morphology and continuity of the endothelial layer and the basement membrane, the capillary endothelium can be divided into continuous, fenestrated, and discontinuous endothelium.

Tight junctions between endothelial cells and underlying uninterrupted basement membrane characterize the continuous endothelium, through which the passage of polymeric molecules is greatly hampered (see Figure 5, situation 1). Such type of endothelium characterizes the skeletal, cardiac, and smooth muscles, and can be found in lung, skin, and subcutaneous tissues. Dendrimeric and other polymer-based nanoparticles with diameters equal or greater than 6 nm hardly interact with parenchymal cells in these tissues, simply because of the barriers posed by the endothelium. Endothelial cells having fenestrae featuring a diaphragm – an opening 40–80 nm in diameter – form the fenestrated endothelium found in the intestinal mucosa, the endocrine and exocrine glands, and the glomerulus and peritubules of the kidney (see Figure 5, situation 2). However, the passage of macromolecules through this type of endothelium is limited by the presence of the basement membrane. The discontinuous (or sinusoidal) endothelium is found only in the liver, spleen, and bone marrow. These capillaries are characterized by endothelial gaps, intracellular junctions with a diameter up to 30–500 nm and with either no basement membrane (liver) or a discontinuous basement membrane (spleen and bone marrow). Therefore, parenchymal cells in these tissues can be accessed by macromolecules with relatively high molecular weight and, consequently, large dimensions (see Figure 5, situation 3). A similar situation (i.e., big fenestrations and enhanced vascular permeability of nanoparticle-based drug delivery systems) are also found in several solid tumors.

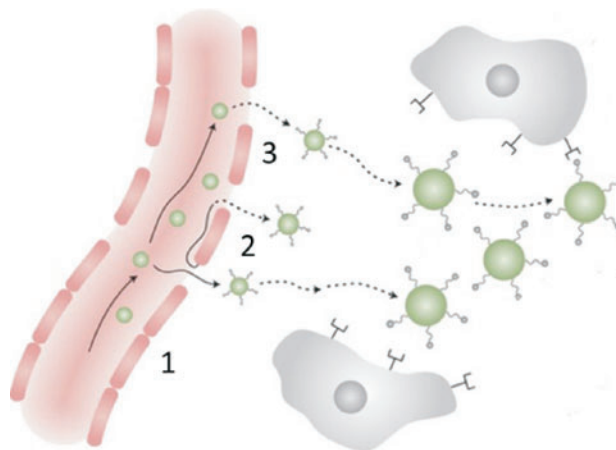


Fig. 5 – The concept of nanoparticle extravasation from different endothelial junctions/fenestrations

According to the above discussion the size and, hence, the structure of dendrimers as a function of pH is a critical issue for their utilization as drug delivery vehicles in physiological environments (pH = 7.4). Molecular simulations can provide insights into the structure and the properties of dendrimers as a function of generation by yielding, for instance, the values of the radius of gyration R_g and the corresponding radial distribution functions of the dendrimers via fully atomistic MD simulations in explicit solvent, counterions, and ionic strength.

The radius of gyration R_g is related to the square root of the second invariant of the first order tensor S , and takes into account the spatial distribution of the atom chain by mediating over all N molecular components. For a dendrimer, the mean-square radius of gyration is defined by:

$$\langle R_g^2 \rangle = \frac{1}{M_w} \left\langle \left[\sum_{i=1}^N m_i |r_i - R|^2 \right] \right\rangle \quad (1)$$

where R is the center of mass of the dendrimer, r_i and m_i are the position and mass of the i th atom, and M_w refers to the total mass of the dendrimer. The R_g values estimated by MD simulations for ethylenediamino (EDA)-core PAMAM dendrimers of generation 1 to 6 (G1-G6) are shown in Figure 6 as a function of the dendrimer M_w and listed in the third column of Table 1 as a function of the dendrimer generation G . As can be seen from these data, the dimensions of these nanocarriers increase linearly with M_w ; also, their overall dimensions are such that, according to the above discussion, their extravasation can easily take place through the fenestrated endothelium and even through the endothelial cells tight junctions. Importantly, these values are in excellent agreement with those previously determined by SAXS experiments, and with other MD simulations, as evidenced in Table 1.

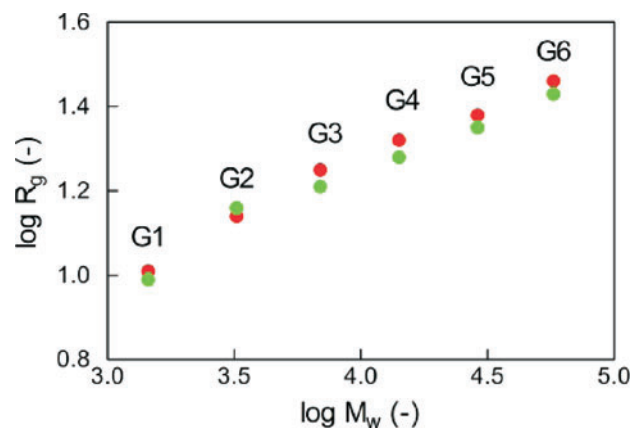


Fig. 6 – Log-log plot of R_g calculated from MD simulations as a function of the PAMAM molecular weight. Green symbols, pH = 7.4; red symbols, pH = 5. From PAMAM dendrimers for siRNA delivery: computational and experimental insights, Pavan, G.M.; Posocco, P.; Tagliabue, A.; Maly, M.; Malek, A.; Danani, A.; Ragg, E.; Catapano, C.V.; Pricl, S. *Chemistry Eur. J.* 16(26), Copyright © [2010], John Wiley & Sons, <http://onlinelibrary.wiley.com/doi/10.1002/chem.200903258/pdf>.

It is interesting at this point to recall that the internalization and accumulation of PAMAM-NH₂ dendrimers in the cellular endosomes result in the acidification of the overall environment. As a consequence, protonation of the dendrimers tertiary amine nitrogens takes place as a buffering mechanism, which triggers the diffusion and accumulation of Cl⁻ counterions into the endosomes. These, in turn, results in an increased endosomal osmotic pressure and eventually rupture of the endosomal membrane and release of its contents, including the loaded dendrimers, into the cytoplasm of the targeted cells. As shown in Figure 1 and Table 1, and as expected, the dimensions of the PAMAMs increase with increasing generation and, coherently, the R_g values at lower pH (e.g., pH = 5) are greater than the corresponding values at pH = 7.4 by virtue of the protonation of the tertiary amine nitrogen at

Table 1 – Radius of gyration R_g values (Å) for PAMAM dendrimers obtained from MD simulations at two different pH values (standard deviation in parenthesis). For comparison, experimental values obtained through SAXS experiments and theoretical values derived from previous MD simulations are given. From PAMAM dendrimers for siRNA delivery: computational and experimental insights, Pavan, G.M.; Posocco, P.; Tagliabue, A.; Maly, M.; Malek, A.; Danani, A.; Ragg, E.; Catapano, C.V.; Pricl, S. *Chemistry Eur. J.* 16(26), Copyright © [2010], John Wiley & Sons, <http://onlinelibrary.wiley.com/doi/10.1002/chem.200903258/pdf>.

Generation	pH = 5	pH = 7.4		SAXS ¹⁵		Other MD simulations ¹⁶
G1	10.19 (0.34)	9.85 (0.30)				
G2	13.88 (0.37)	14.44 (0.41)				
G3	17.96 (0.17)	16.25 (0.38)	15.8 ^[a]	16.5 ^[b]	15.09 ^[b]	
G4	21.00 (0.22)	19.00 (0.21)	17.1	17.6	18.6	16.78 ^[c]
G5	24.23 (0.18)	22.43 (0.29)	24.1	25.3	23.07	20.67
G6	28.90 (0.10)	27.21 (0.11)	26.3	27.5	27.5	26.76

^[a]In CH₃OH from sphere model. ^[b]In CH₃OH from Guinier plot. ^[c]In explicit water and counterions.

oms which, in turn, leads to a molecular expansion by internal charge repulsion. This allows for an enhanced water and counterions penetration into the dendrimer branches, with the ultimate consequence of nanovector swelling. This behavior is commonly known as the *proton sponge effect*, as the influx of water and chlorine counterions to compensate the increased protonation state of the dendrimer makes the nanocarriers behave like a virtual proton sponge.

Another substantial effect of the degree of protonation of cationic dendrimers (such as PAMAMs) for nucleic acid delivery is that, by lowering the pH and, hence, increasing the dendrimer protonation level, more counterions are expected to move inside the dendrimer, resulting in an ultimate greater dendrimer swelling. Figures 7a and 7b plot the radial density distributions of all PAMAM generations at low and neutral pH, respectively. It can be inferred that, in presence of solvent and both at neutral or low pH, for G1–G6 the density distribution is characterized by a maximum at small R values, and then decreases somewhat monotonically with increasing R . This effect becomes more evident as the pH decreases, and constitutes an indication that the dendrimer core region is denser than the outer part. Because of this hollowness at the middle regions of the molecule, a significant number of water molecules are allowed to penetrate within the dendrimer inner branches.

A further, peculiar feature of dendrimeric structures which may affect their performance as nanocarriers is the high degree of back-folding. The usual schematic diagrams found in the literature for dendrimers, particularly the 2D representations, convey the idea that the terminal groups are located at the periphery of the molecule. However, the actual MD simulations reveal the presence of a substantial back-folding of the end groups toward the dendrimer core. To quantify this aspect, the radial distribution functions for terminal nitrogens for various generations are reported in Figures 7c and 7d. This indicates that the end groups are sufficiently flexible to interpenetrate nearly the whole molecule. In particular, the end groups of higher generations come even close to the core of the molecule, and the extent of back-folding increases with the increase of generation. This effect is again more evident at neutral pH; higher generations show evident peaks near the core of the molecule and, for smaller generations, the back-folding pervades the entire molecular architecture. Obviously, the presence of a substantial backfolding is detrimental to NA binding, as less protonated terminal groups are available on the dendrimer surface; accordingly, the overall dendrimer surface charge is diminished, the corresponding ionic interactions with the NA is lower,

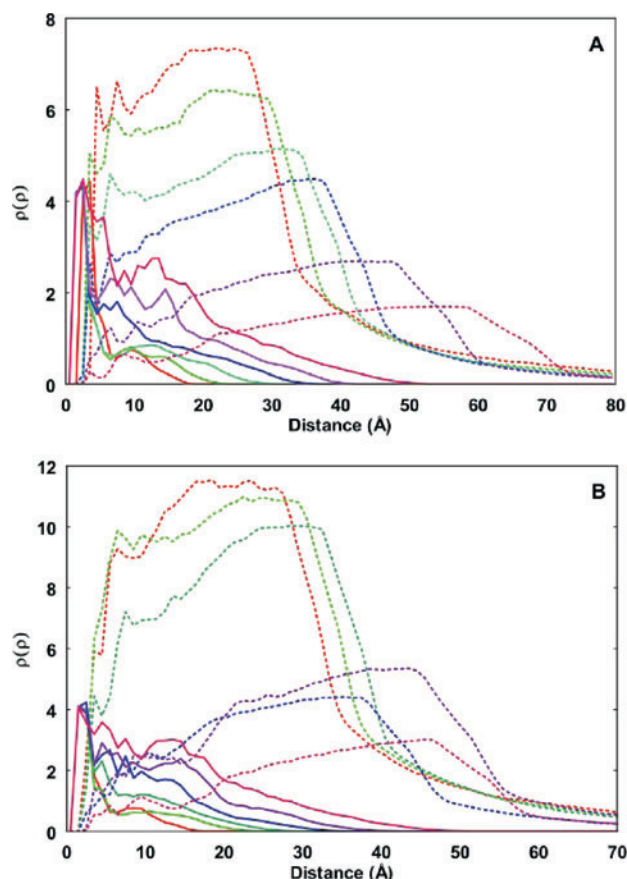


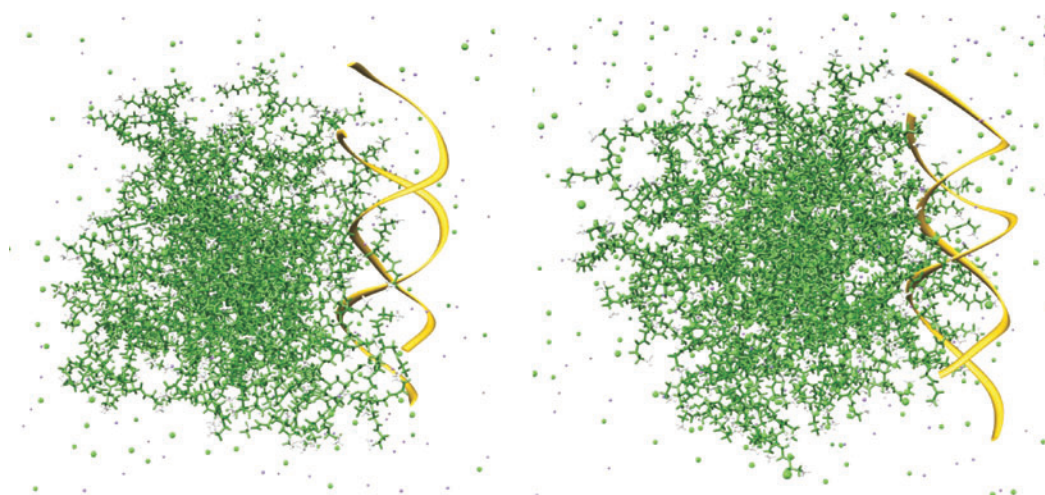
Fig. 7 – Radial density distributions for PAMAM generations G1 to G6 (continuous lines) and water (broken lines) at pH = 5 (a) and pH = 7.4 (b). Radial density distributions for terminal nitrogens of PAMAM generations G1 to G6 at pH = 5 (c) and pH = 7.4 (d). Color legend: red, G1; light green, G2; dark green, G3; blue, G4; purple, G5; dark red, G6. From PAMAM dendrimers for siRNA delivery: computational and experimental insights, Pavan, G.M.; Posocco, P.; Tagliabue, A.; Maly, M.; Malek, A.; Danani, A.; Ragg, E.; Catapano, C.V.; Pricl, S. *Chemistry Eur. J.* 16(26), Copyright © [2010], John Wiley & Sons, <http://onlinelibrary.wiley.com/doi/10.1002/chem.200903258/pdf>.

and the NA cargo might be lost along the way to the target cell under the action of drag forces in the blood stream or the uptake of plasma proteins. On the other hand, a too strong interaction between the nanovector and its cargo can turn out to be unfavorable in a later stage of the delivery process, that is during NA release in the cell cytoplasm: a tight electrostatic bond between the two molecular entities may disfavor the NA detachment from its vector, thus making the NA unavailable for further, therapeutic action.

But how about dimensions when the dendrimeric nanovector and its nucleic acid cargo complex and form a dendriplex? Once again, to try to find an answer to this crucial question we can resort to computer-assisted simulations and characterize the conformational change of dendrimer and the nucleic acid upon binding by calculating the values of

Table 2 – Radius of gyration values R_g^{compl} (Å) for G4–G6 PAMAM dendrimers in complex with a 21 base-pairs RNA fragment (standard deviations in parenthesis). The values for the dendrimer and siRNA within the corresponding complexes, R_g^{dend} and R_g^{NA} , are also given. Adapted from PAMAM dendrimers for siRNA delivery: computational and experimental insights, Pavan, G.M.; Posocco, P.; Tagliabue, A.; Maly, M.; Malek, A.; Danani, A.; Ragg, E.; Catapano, C.V.; Pricl, S. *Chemistry Eur. J.* 16(26), Copyright © [2010], John Wiley & Sons, <http://onlinelibrary.wiley.com/doi/10.1002/chem.200903258/pdf>.

Generation	pH = 5			pH = 7.4		
	R_g^{compl}	R_g^{dend}	R_g^{siRNA}	R_g^{compl}	R_g^{dend}	R_g^{siRNA}
G4	23.65 (0.15)	22.06 (0.15)	19.56 (0.39)	23.01 (0.21)	19.56 (0.24)	20.08 (0.36)
G5	25.83 (0.10)	24.76 (0.10)	18.79 (0.33)	24.81 (0.14)	23.47 (0.15)	20.41 (0.21)
G6	30.01 (0.14)	29.38 (0.08)	19.76 (0.35)	28.39 (0.07)	27.41 (0.08)	19.43 (0.33)



the radius of gyration of the entire complex, R_g^{compl} , and those of the dendrimer and the NA within the complex, R_g^{dend} and R_g^{NA} , respectively. As an example, Table 2 shows the relevant values again for PAMAM dendrimers in complex with a RNA fragment of 21 base-pairs. At both pH values and for each dendrimer generation, R_g^{NA} is significantly smaller than R_g^{dend} , testifying the tendency of the NA fragment to partially penetrate inside the dendrimeric structure. Nevertheless, as expected, the biggest part of the NA double helix still remains outside the dendrimer, and this reflect in a R_g^{compl} value being larger than R_g^{dend} . Furthermore, the NA is a duplex many therapeutic NAs are in a duplex form, and the base pairing/stacking interactions between the opposite strands concur to confer an intrinsic rigidity to the overall structure, preventing a substantial wrapping of the nucleic acid around the dendrimer surface (see Figure 8).

Comparing Figure 9a and 9b, it can be seen that, due to the swelling of the polymer, considerable water can penetrate inside the dendrimer. The water uptake seems to be dependent on dendrimer generation; in particular, at neutral pH, water diffusion within the dendrimer branches decreases as G increases. In any case, water molecules are detected even close to the dendrimer cores at both pHs.

Upon NA complexation, all PAMAM generations do not appear to undergo major conformational changes, maintaining the dense core configuration observed for isolated dendrimers (see Figures 7a and 7b). Finally, the NA density distributions are found well inside the corresponding dendrimer density profiles, indicating that the nucleic acid can easily penetrate into the outmost dendrimer branches, some base pairs reaching deeper into the nanovectors structure. In concluding this section, it is important to remark that also the dendriplexes formed by G1–G6 PAMAMs as nanocarriers and small fragments of NA, as are the so-called small-interference RNA (siRNA),⁴ still possess dimension fully compatible with easy extravasation through all types of endothelium.

Nano dimensions, mega interactions

Indeed, the ability of a nanocarrier to generate a stable complex with its nucleic acid payload is a background postulate for its usefulness in gene delivery. This property can be experimentally explored and quantified through the use of many disparate techniques, ranging from the standard Ethidium Bromide (EthBr) displacement fluorescence spectroscopy assay to the more sophisticated

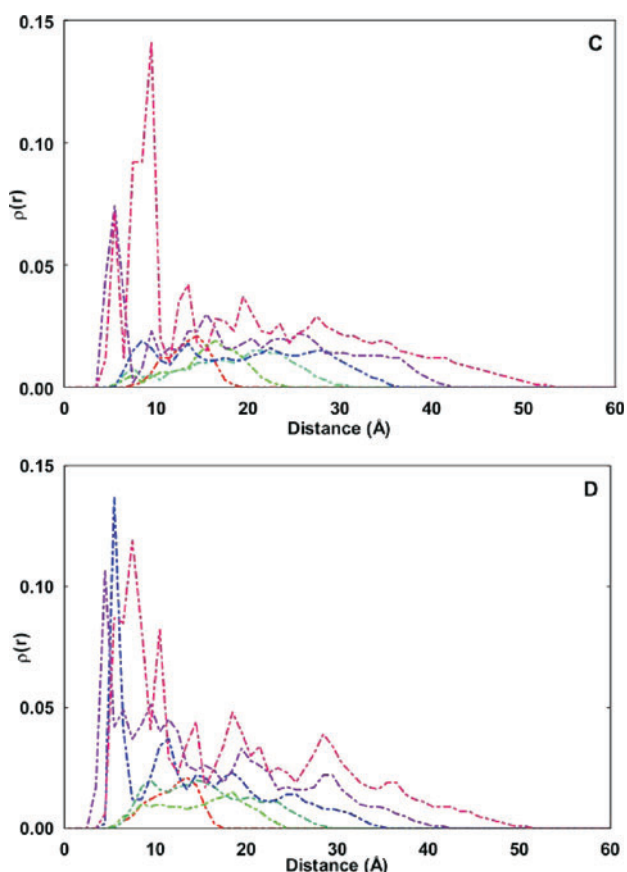


Fig. 8 – Snapshots taken from MD simulations of PAMAM generations G6 in complex with GL3 siRNA at different protonation levels. Top: low pH (= 5) structure; bottom: neutral pH (= 7.4) structure. Dendrimers are depicted in colored sticks representation, with the terminal NH_3^+ groups highlighted as white sticks-and-balls. The siRNA is outlined as a golden ribbon. Sodium and chlorine counterions are portrayed as purple and green sphere, respectively. Water is omitted for clarity. From PAMAM dendrimers for siRNA delivery: computational and experimental insights, Pavan, G.M.; Posocco, P.; Tagliabue, A.; Maly, M.; Malek, A.; Danani, A.; Ragg, E.; Catapano, C.V.; Pricl, S. *Chemistry Eur. J.* 16(26), Copyright © [2010], John Wiley & Sons, <http://onlinelibrary.wiley.com/doi/10.1002/chem.200903258/pdf>.

and quantitative isothermal titration calorimetry (ITC) or differential scanning calorimetry (DSC). Multiscale molecular simulations, however, not only can yield the same information in a less expensive way (both from time and money standpoint), but may offer a reliable molecular rationale to explain the generation, structural, ionic strength, and other chemico-physical properties and mechanisms determining the dependence of the affinity of a given dendrimer/dendron carrier to its nucleic acid cargo. This can be easily understood looking at Table 3, in which the free energy of binding (ΔG_{bind}) between PAMAMs from generation G4 to generation G6 and a short fragment of double-stranded (ds) RNA is listed, together with its major components (i.e., the enthalpic contribution ΔH_{bind} , and

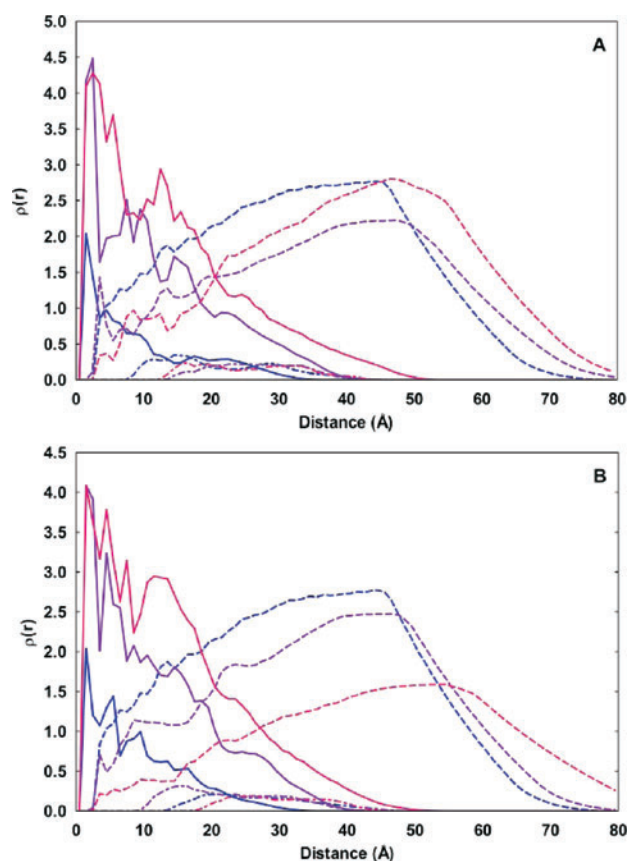


Fig. 9 – Radial density distributions for PAMAM generations G4 to G6 in complex with siRNA (continuous lines), water (broken lines), and siRNA (dotted-broken line) at pH = 5 (A) and pH = 7.4 (B). Color legend: blue, G4; purple, G5; dark red, G6. From PAMAM dendrimers for siRNA delivery: computational and experimental insights, Pavan, G.M.; Posocco, P.; Tagliabue, A.; Maly, M.; Malek, A.; Danani, A.; Ragg, E.; Catapano, C.V.; Pricl, S. *Chemistry Eur. J.* 16(26), Copyright © [2010], John Wiley & Sons, <http://onlinelibrary.wiley.com/doi/10.1002/chem.200903258/pdf>.

the entropic term $-\text{T}\Delta S_{\text{bind}}$, see Supporting Information for more details)). As it can be seen from this table, the affinity for all three dendrimer generations for the NA is very high, and increases with increasing G , as expected.

As expected for the interaction of two highly, oppositely charged macroions, the electrostatic part of the nonbonded mechanical energy components of ΔG_{bind} , ΔE_{ele} , affords the predominant contribution to binding for each dendrimer generation and at both pH values. On the other hand, due the polar character of both nanovectors and cargo, the desolvation penalty paid by these molecules upon binding (ΔG_{PB}) is also quite substantial. The corresponding mean values of the van der Waals and hydrophobic overall interaction energies ($\Delta E_{\text{vdW}} + \Delta G_{\text{NP}}$, see Table 3) amount approximately to 10% of the overall electrostatic components ($\Delta E_{\text{ele}} + \Delta G_{\text{PB}}$), thus confirming the substantial electrostatic nature of the interactions in the dendriplexes.

Table 3 – Free energy of binding and its component for the formation between PAMAM G4, G5, and G6 and a small fragment (21 base-pairs) of RNA under two pH conditions of physiological interest as obtained from MM/PBSA calculations at $T = 300\text{K}$. All values are in kcal/mol. Standard errors of the means are reported in parenthesis.

	pH = 7.4			pH = 5.0		
	G4/RNA	G5/RNA	G6/RNA	G4/RNA	G5/RNA	G6/RNA
ΔE_{vdW}	-44.58 (5.93)	-66.50 (9.70)	-71.29 (9.18)	-87.18 (9.49)	-114.57 (13.18)	-135.77 (15.22)
ΔE_{ele}	-27186.60 (210.40)	-51796.44 (364.56)	-86827.58 (1493.61)	-57630 (619.27)	-100315.04 (678.29)	-158934.28 (2382.03)
ΔE_{MM}	-27231.18 (209.94)	-51862.94 (364.32)	-86898.88 (1500.45)	-57717.68 (624.39)	-100429.61 (689.07)	-159070.05 (2398.29)
ΔG_{NP}	-11.12 (0.57)	-17.56 (1.39)	-15.21 (1.78)	-20.14 (1.97)	-24.46 (1.94)	-26.33 (1.91)
ΔG_{PB}	26870.38 (203.46)	51227.80 (354.70)	85901.50 (1480.93)	56985.10 (603.46)	99307.69 (682.91)	157252.06 (2292.85)
ΔH	-371.92 (13.71)	-652.69 (13.85)	-1012.59 (29.70)	-752.72 (27.97)	-1146.38 (35.81)	-1844.32 (31.78)
$-\text{T}\Delta\text{S}$	+64.78 (3.64)	+101.64 (13.14)	+228.79 (25.64)	+154.47 (16.74)	+284.42 (29.23)	+577.06 (56.88)
ΔG_{bind}	-307.14	-551.05	-783.80	-598.25	-861.96	-1267.26

Interestingly, a least-squares linear regression fit of the values of ΔH_{bind} versus $-\text{T}\Delta\text{S}_{\text{bind}}$ listed in Table 3 (correlation coefficient $R^2=0.98$) demonstrates the linear relationship between the enthalpies and the entropies of RNA binding to the PAMAMs (Figure 10a). As this plot indicates, the binding entropy decreases when the binding enthalpy increases. One explanation for this observation is that as the dendrimer forms favorable interactions by wrapping the small RNA fragment with some of its outer branches, both the dendritic arms and the nucleobases involved in these interactions lose degrees of freedom upon binding. Moreover, solvent molecules and stabilizing counterions associated with the hydration shell of the nanovector and those residing in the binding pocket in the major groove of the siRNA also become rearranged. Similarly, a plot of ΔH_{bind} vs. ΔG_{bind} (shown in Figure 10b) is also linear ($R^2=0.99$), again characteristic of classical enthalpy/entropy compensation.

The role of solvation in gene binding by nanovectors

Soft colloids and macromolecules with flexible structures and void pervading their entire complex molecular structure are necessarily hydrated not only in their outer shell. Indeed, ions and water can penetrate along the tortuous pathways of holes and channels of the macromolecular entity, eventually reaching down to the inner core. In harmony with the foregoing discussion of the propensity of dendrimers to swell in water (particularly at low pH) and of the role of the conformational and chemico-physical features of a given dendrimers in the corresponding ability to adapt to an environ-

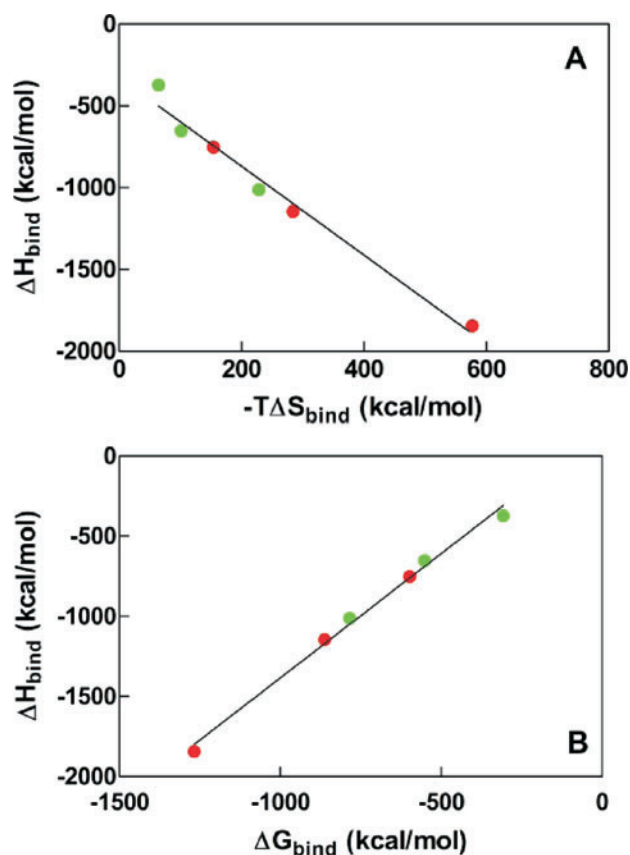


Fig. 10 – Relationship between the enthalpy and the entropy of siRNA binding to G4–G6 PAMAM dendrimers at two different pH: 7.5 (green symbols) and 5 (red symbols). A) Plot of ΔH versus $-\text{T}\Delta\text{S}$ and B) plot of ΔH versus ΔG_{bind} . The two solid lines through the data are the best fit lines (see Table 3). From PAMAM dendrimers for siRNA delivery: computational and experimental insights, Pavan, G.M.; Posocco, P.; Tagliabue, A.; Maly, M.; Malek, A.; Danani, A.; Ragg, E.; Catapano, C.V.; Priel, S. *Chemistry Eur. J.* **16**(26), Copyright © [2010], John Wiley & Sons, <http://onlinelibrary.wiley.com/doi/10.1002/chem.200903258/pdf>.

mental change, Figure 11 shows the swelling capacity of a triethanolamine (TEA)-core PAMAM as obtained from computer simulations: indeed, in this case the presence of a large core in the dendrimeric structure favors the penetration of a high amount of water molecules within the dendrimer interior (compared to the EDA-core PAMAMs, see previous paragraph), particularly at high generations and low pH (both fundamental parameters for efficient delivery); moreover, the number of intra-dendrimer water molecules grows almost linearly with pH.

Upon binding of the dendrimer to the nucleic acid, water plays even more determining roles. First, it creates a bridge between the carrier and the DNA/RNA, by maintaining an hydration layer and ensuring the instauration of a hydrogen bond network between the carrier and the nucleic acid, critical to their complex formation and stability. More important, perhaps, is the role of overall solubilization. Water and the solution navigating salts must pervade the entire system to guarantee uniform hydration and dispersion of the loaded

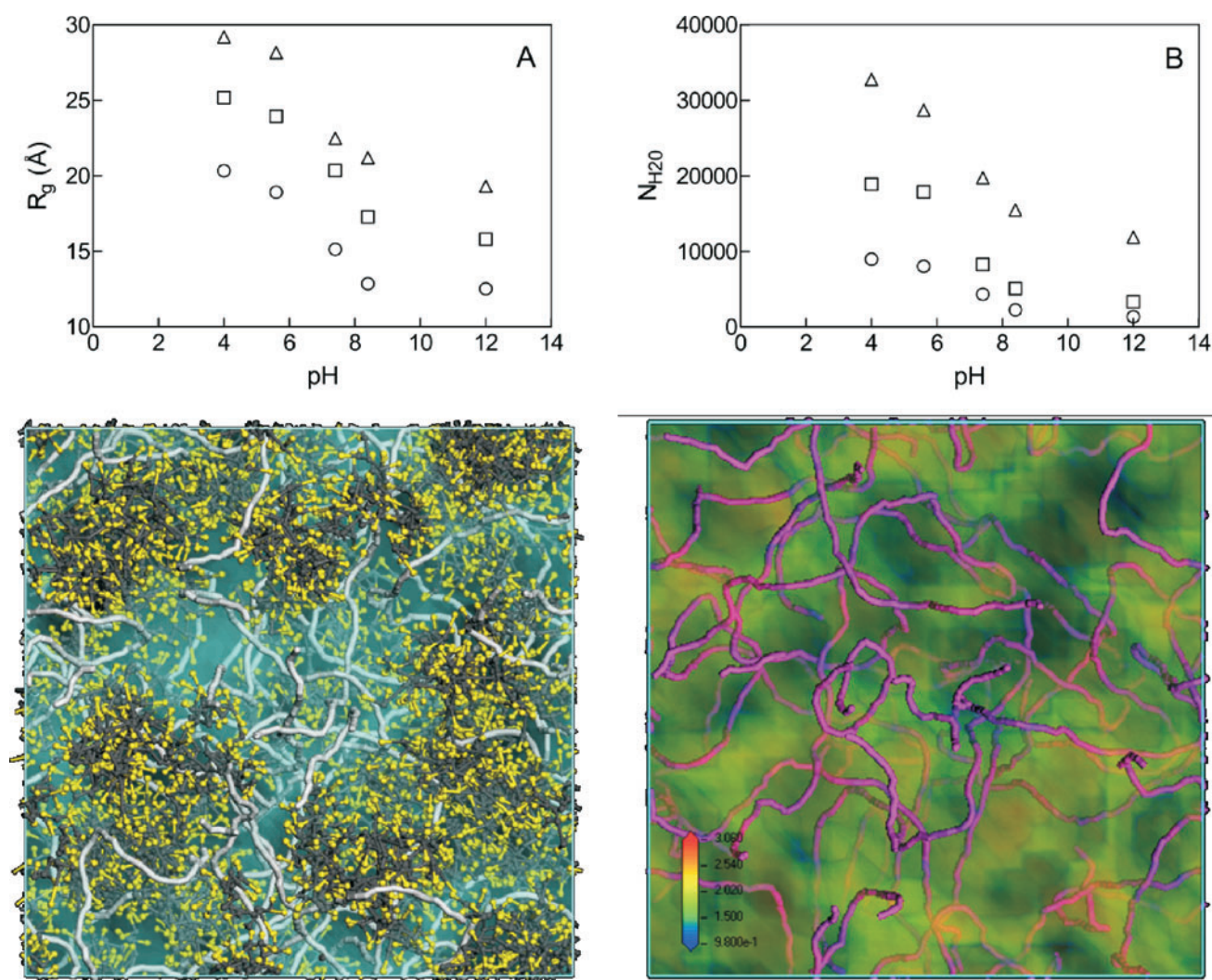


Fig. 11 – (a) Radius of gyration R_g as a function of the solution pH for G4-G6 TEA-core PAMAMs in complex with a small fragment of double-stranded RNA. (b) Number of water molecules in the G4-G6 TEA-core PAMAM dendrimer interiors as a function of the solution pH. Symbol legend: circles, G4; squares, G5; triangles, G6. Error bars are smaller than symbols. Reproduced from *Poly(amidoamine)-based dendrimer/siRNA complexation studied by computer simulations: effects of pH and generation on dendrimer structure and siRNA binding*, Karatasos, K.; Posocco, P.; Laurini, E.; Pricl, S., *Macromol Biosci.*, 12(2), Copyright © [2012], John Wiley & Sons, <http://onlinelibrary.wiley.com/doi/10.1002/mabi.201100276/abstract>. (bottom, left) Mesoscale morphologies of the assembled systems between TEA-core dendrimers G6 and DNA. The dendrimers are represented as dark gray and yellow sticks while the DNA is shown as light gray sticks. Water is portrayed as a light gray field. (bottom, right) DNA chains and water molecules distribution within the architectures of the TEA-core DNA/G6 nanoscopic assembly. In this case, water is represented as a colored density field: according to the scale reported in the lower left corners of the panels, blue density values are black, while high density values are white. Adapted with permission Liu, X.X.; Wu, J.; Yamine, M.; Zhou, J.; Posocco, P.; Viel, S.; Liu, C.; Ziarelli, F.; Fermeglia, M.; Pricl, S.; Victorero, G.; Nguyen, C.; Erbacher, P.; Behr, J.P.; Peng, L. Structurally flexible triethanolamine core PAMAM dendrimers are effective nanovectors for DNA transfection in vitro and in vivo to the mouse thymus. *Bioconjug. Chem.*, 2011, 22(12), 2461–2473. Copyright {2011} American Chemical Society.

nanoparticles, avoiding their aggregation and collapse. Mesoscale simulations offer the possibility to predict and study this type of behavior; in fact, a typical result of a mesoscale simulation is the morphology and the structure of matter at nanoscale level at the desired environmental conditions.^{14c)} Let us then consider the lower panels of Figure 11, where the nanoscale morphology of a DNA/G6 complexes of TEA-core dendrimer is presented. As it can be seen from this figure, the TEA dendrimers are able to complex the DNA strands efficiently and homogeneously, with the DNA chains well enwrapped in the systems and the absence of DNA bundles at the nanoscopic level. Further, the water density maps at the mesoscopic level not only support the lower-scale (i.e., atomistic MD) results discussed above of a higher degree of hydration but also confirm the uniform water molecule distribution within the nucleic acid/TEA-core PAMAM dendrimer.

From a structure-activity relationship (SAR) standpoint, the enhanced swelling capacities of the TEA-core dendrimers at low pH values may result in a higher buffering capacity which, in turn, can be beneficial to endosomal escape of the nucleic acid cargo via the proton sponge effect. At the cellular level, in fact, inadequate cytosolic access is one major challenge that must be overcome if nanovector/DNA(RNA) systems are to become effective *in vivo* therapeutics. The increased swelling and, possibly, the increased proton sponge effect of more flexible and open structure dendrimers such as the TEA-core PAMAMs undoubtedly concur to enhance the capacity of these nanovectors and their cargoes to enter the endosome, adsorb protons, swell and cause an influx of negative (e.g., Cl⁻) counterions which, in turn, creates an osmotic effect ultimately leading to water uptake. This escalation of events are purported to cause endosome membrane destabilization and rupture, with subsequent release of the nanodelivery complex in the cellular cytosol. Thus, should the proton sponge effect be the operative mechanism underlying endosome escape of the nanovector and release of its payload, then flexibility, softness, and conformational freedom are all key molecular parameters in a dendrimer-based nanocarrier.

Multivalency in gene delivery

Multivalent systems are widely found in nature, and especially in biology: adhesion of viruses or bacteria to cells' surface, cell to cell adhesion, and cell to polyvalent molecule interactions. A good example of multivalency resides in the defense process of the immune system involving bacteria, antibodies, and macrophages. Antibodies

have the ability to recognize *non-self* entities, such as bacteria, upon polyvalent binding with antigens, or other proteins, located at their surface. It is noteworthy that weak ligand-receptor interactions can be made much stronger simply by the simultaneous bonding of these ligands to these multiple receptors.

High-affinity molecular recognition of biomolecular targets is of crucial importance in the development of synthetic systems capable of intervening in biological pathways; multivalent recognition is a key principle in enhancing binding strength and hence developing systems with potential biomedical applications. Experimental studies and mathematical models have demonstrated that once the first ligand in a multivalent array has bound to the target, the binding of a second ligand is usually a cooperative, entropically less disfavored process, with a local concentration effect also enhancing binding.

Dendrimers and dendrons are inherent multivalent ligands that can present multiple recognition elements from a central scaffold. The scaffold plays a crucial role because it molds the final architecture in term of shape, orientation of recognition elements, flexibility, size and valency. When the multiple surface groups are ligands, the dendritic scaffolding can be considered to act as a kind of nanoscaffolding, organizing the ligand array. As such, dendritic systems have been widely exploited for their potential applications in multivalent biological recognition. ,

Self-assembly is an incredibly powerful concept in modern molecular science. The ability of carefully designed building blocks to spontaneously assemble into complex nanostructures underpins developments in a wide range of technologies, from materials science to molecular biology. Self-assembly is a supramolecular approach which relies on complementary noncovalent interactions, such as electrostatic and van der Waals forces, hydrogen bonds, coordination interactions and solvophobic effects. In self-assembled structures, these temporal intermolecular forces connect to the molecular scale building blocks in a reversible, controllable, and specific way. Of particular value are the possibilities offered by self-assembly to generate nanoscale complexity with relatively little synthetic input. Furthermore, the ability of self-assembled superstructures to behave as more than the sum of their individual parts, and exhibit completely new types of behavior, is of special interest and appealing in (bio)nanotechnology.

There are a number of different ways in which dendrimers or dendrons can be assembled in solution; perhaps the most efficient approach is the one

that gives rise to well-defined (i.e., monodisperse) assemblies of dendritic building blocks. The supermolecular structures generated using this approach are generally based on well-established, specific intermolecular interactions; consequently, each assembly contains a defined number of dendritic building blocks. Such supermolecular dendrimeric structures have an equivalent degree of structural definition to a traditional covalent dendrimer; however, they are held together by reversible, nonbonded interactions. Given the relative simplicity of using self-assembly as a noncovalent synthetic tool, this approach is relatively cost-effective, and its potential for genuine future applications is therefore significantly enhanced.

Surface-active amphiphilic molecules are well-known to assemble into discrete structures such as micelles and vesicles in water solution. Amphiphilic dendritic systems are not exception to this rule, and a range of dendrimers with surfactant-like assembly properties have been reported. Indeed, when mixed with water, the apolar and polar regions of these Janus-type molecules will attempt to phase separate via self-assembly into structures such as micelles. Importantly, only in some cases does the aggregation process give rise to true micellar structures: this occurs at molecular concentrations C greater than the so-called critical micellar concentration (CMC), which is one of the key parameter in self-assembly. When $C > \text{CMC}$, aggregates with a variety of different, non-micellar structures – often ill-defined – are formed. In other words, CMC defines the thermodynamic stability of the micelles. The latter is a very critical property in drug-delivery applications of micelles because intravenous injection of micellar solutions are associated with extreme dilutions by circulating blood (usually about 25-fold dilution at bolus injection or a much higher dilution at infusion). If the concentration of a micelle forming molecule in the circulation drops below the CMC, the micelles may be prematurely destroyed, resulting in the release of their cargo into the bloodstream before it reaches its target. This, in turn, will not only result in a poor therapeutic regime but, perhaps more importantly, could be dangerous because off-target and other unwanted side effects might (and likely will) originate. On the other hand, amphiphilic compound concentration cannot be increased above some critical values that correspond to the onset of micellar aggregation and precipitation, provoked by the interpenetration of the hydrophilic micellar coronas.

Under these perspective, our group recently synthesized a series of dendrons with a variety of lipophilic units at their focal points (see Figure 12) and tested these molecules for DNA binding and

cell transfection capacities, revealing a set of stimulating evidences: not only all modified dendrons were able to tightly bind DNA and efficiently transfect cells, but for the first time and with the aid of multiscale molecular modeling a structure-activity relationship (SAR) could be formulated between the DNA binding affinity and the overall surface charge σ_m of the micellar assemblies but, perhaps more importantly, the SAR could be extended to cellular gene delivery, as σ_m plays a fundamental role in controlling the extent of the endosomal escape (*vide infra*).^{13a}

Thus, state-of-the-art multiscale simulation techniques were employed to monitor the dendrons self-assembly processes and to gain an insight into the types of aggregates eventually formed. First of all, the simulations revealed that all hydrophobically modified dendrons of generation 1 were able to form spherical supermolecular structures (see Figure 13) with diameters D_m in the range of 3 – 5 nm (see Table 4).

The spherical geometry of the self-assembled supramolecular entities is a direct consequence of the conical molecular shape of each dendron, featuring a relative large cationic head and a comparatively small lipophilic part. In fact, assembly geometries for amphiphilic molecules is dictated by the proportions of their polar and apolar domains, aptly described by the so-called packing parameter $P = v_h/a_0l_c$, in which v_h is the volume of the densely packed hydrophobic segment, a_0 is the effective cross-sectional area of the hydrophilic group, and l_c is the chain length of the hydrophobic moiety normal to the interface. Based on simple geometric considerations of micellar core volume vs. surface area, it is easy to show that $P < 1/3$ is characteristic of spherical micelles, $1/3 < P < 1/2$ characterizes self-assembly of cylindrical shape, $1/2 < P < 1$ corresponds to vesicles, flat lamellae are formed at $P = 1$ and, lastly, inverted micelles are expected for $P > 1$.

With these rules for P value calculations in mind, let us consider a generic micelle with a core radius R_c , and made up of N_{agg} molecules. By simple geometrical principles, then, the volume V_c of the micellar core can be obtained as $V_c = N_{\text{agg}} v_h = 4\pi R_c^3/3$, the surface area of the core as $A_c = N_{\text{agg}} a_0 = 4\pi R_c^2$ and, finally, the value of the micellar core radius as $R_c = 3 v_h/a_0$. If the micellar core is densely packed with the hydrophobic moieties filling the entire space, then the radius of the micelle core cannot exceed the fully extended length of the hydrophobic portion. Introducing this constraint into the expression for R_c , we then arrive at the above stated condition $0 \leq P \leq 1/3$ if an amphiphile is to form a spherical micelle.

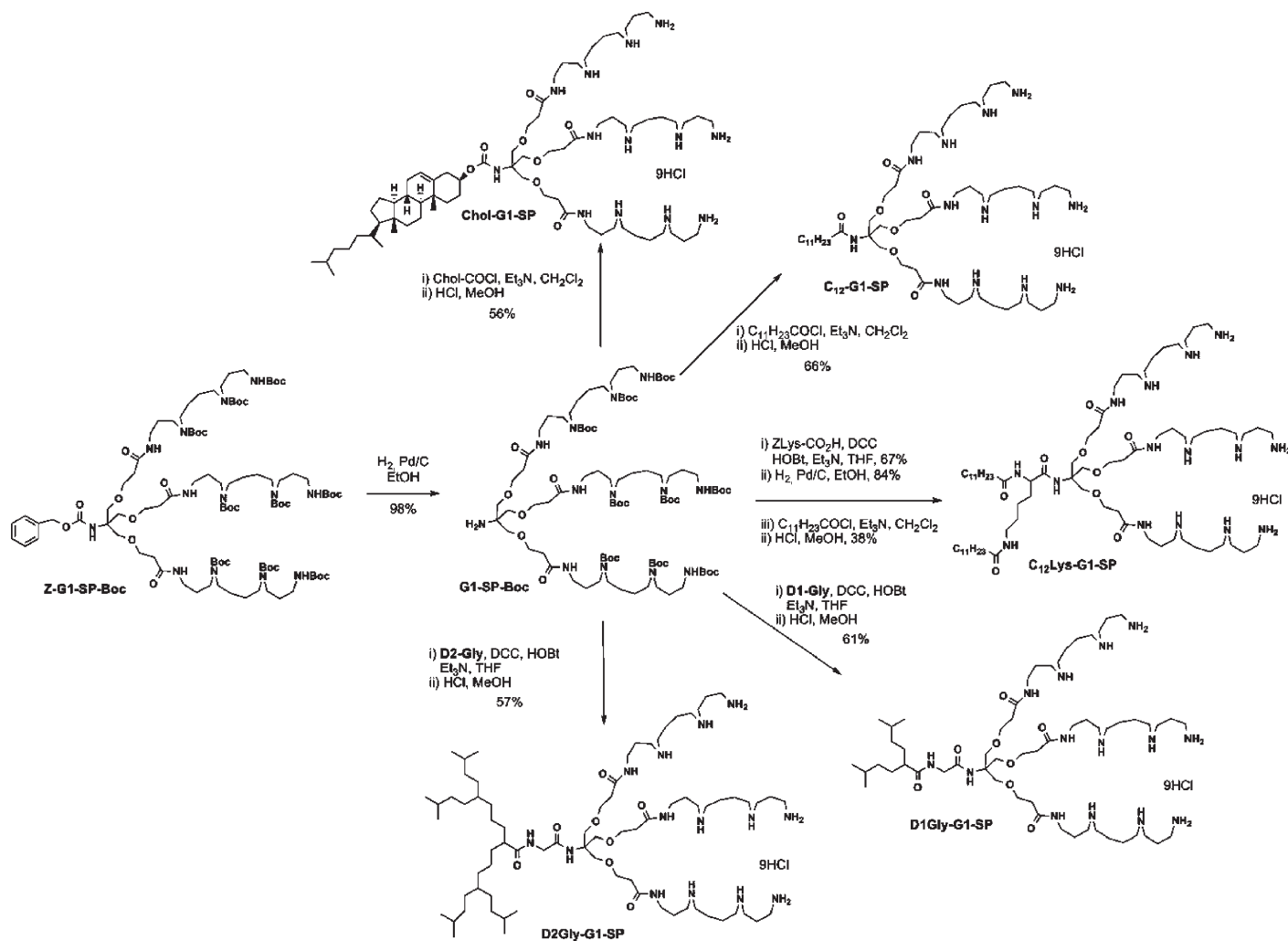


Fig. 12 – Synthetic pathway of first generation dendron-based nanovectors with different hydrophobic groups at the focal point. Reprinted with permission from Jones, S.P.; Gabrielson, N.P.; Wong, C.H.; Chow, H.F.; Pack, D.W.; Posocco, P.; Fermeglia, M.; Pricl, S.; Smith, D.K. *Hydrophobically modified dendrons: developing structure-activity relationships for DNA binding and gene transfection. Mol Pharm.*, 2011, 8(2), 416–429. Copyright {2012} American Chemical Society.



Fig. 13 – Mesoscale modeling of amphiphilic dendrons showing aggregation into spherical micellar objects. (Left) Chol-G1-SP; (middle) C₁₂-G1-SP; (right) D₂Gly-G1-SP. In all pictures, the yellow sticks represent the dendron head groups while colored spheres are adopted to portray the various hydrophobic regions. The gray field is finally used to represent water. Reprinted with permission from Jones, S.P.; Gabrielson, N.P.; Wong, C.H.; Chow, H.F.; Pack, D.W.; Posocco, P.; Fermeglia, M.; Pricl, S.; Smith, D.K. *Hydrophobically modified dendrons: developing structure-activity relationships for DNA binding and gene transfection. Mol Pharm.*, 2011, 8(2), 416–429. Copyright {2012} American Chemical Society.

Table 4 – Values of the micellar diameter D_m (nm), core radius R_c (nm), aggregation number N_{agg} , packing parameter P , and micelle surface charge density σ_m (e/nm²) for the different modified dendrons (Figure 16) as obtained from mesoscale simulations. Reprinted with permission from Jones, S.P.; Gabrielson, N.P.; Wong, C.H.; Chow, H.F.; Pack, D.W.; Posocco, P.; Fermeglia, M.; Pricl, S.; Smith, D.K. *Hydrophobically modified dendrons: developing structure-activity relationships for DNA binding and gene transfection. Mol Pharm.*, 2011, 8(2), 416–429. Copyright {2012} American Chemical Society.

Compounds	D_m	R_c	N_{agg}	P	σ_m
Chol-G1-SP	3.4 ± 0.1	0.8	21	0.24	5.2
C ₁₂ Lys-G1-SP	4.0 ± 0.2	1.3	24	0.24	4.3
D2Gly-G1-SP	4.9 ± 0.2	1.5	32	0.32	3.8
C ₁₂ -G1-SP	4.0 ± 0.1	1.3	16	0.28	2.8
D1Gly-G1-SP	4.0 ± 0.2	0.9	12	0.25	2.1

By coupling basic molecular modeling concepts to the dimensional micellar parameters estimated by mesoscopic simulations and listed in the first three columns of Table 4, we were able to calculate the corresponding value of packing parameter P for all modified dendrons under hydrated conditions. A cursory glance at the P values in Table 4 reveals that in all cases these numbers fall between 0.24 and 0.32, in agreement with the corresponding spherical morphologies predicted by our mesoscopic simulations.

The mesoscale simulations of these dendron micelles carried out in the presence of DNA neatly show that, in all cases, the overall systems consist of parts of free, unfolded, single-chain DNA that

connect micelles on which a partial amount of DNA has been adsorbed (see Figure 14). In other words, all dendron/DNA complexes present a typical *beads-on-a-string* structure, made of dendron micelles connected by a DNA thread. Importantly, this predicted morphology is supported by detailed AFM studies between G4 PAMAM dendrimers and DNA – indicative that these self-assemblies of dendrons can be considered to be somewhat like covalently bound higher generation spherical dendrimers. These structures are also somewhat reminiscent of the structure of open chromatin, which consists of an array of nucleosome core particles, separated from each other by up to 80 base pairs of linker DNA. However, in clear contrast to the periodic structure of open chromatin, the dendron micelles appear to be distributed in a non-periodic, more irregular way.

Summarizing the overall evidence stemming from the analysis of data in Table 4, as obtained from the application of the multiscale molecular modeling recipe, led to the following, important considerations:

- the overall series of spermine-based amphiphilic dendrons assemble into small, spherical micelles in water and in the presence of physiological ionic strength conditions (150 mM), as experimentally verified for similar systems.
- the different architectures of the hydrophobic portion resulted in differently sized micelles and/or a different number of dendrons per micelle N_{agg} , and, hence, a different micellar surface charge density σ_m .

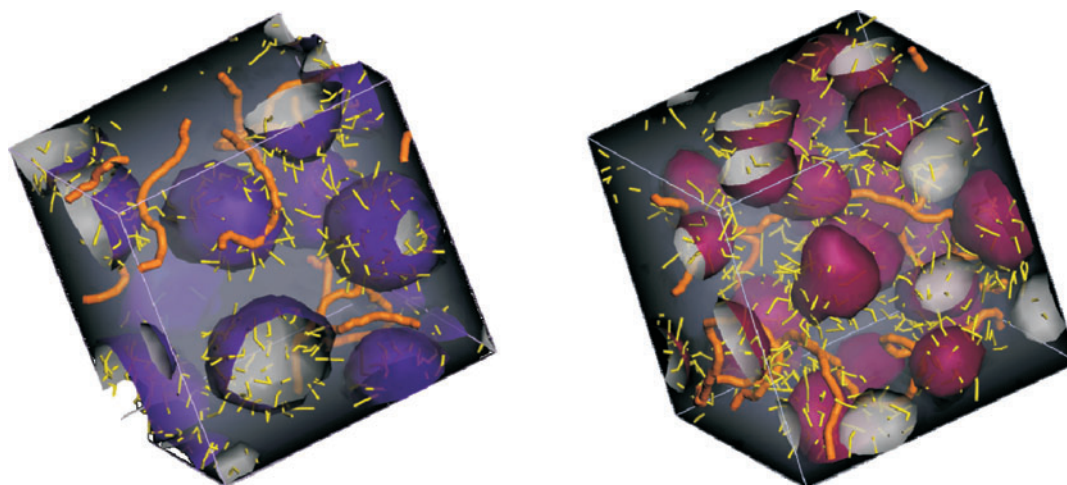


Fig. 14 – Mesoscale modeling of the interaction of DNA with the amphiphilic dendrons D₂Gly-G1-SP (left) and C₁₂-G1-SP (right) as an example. In all pictures, yellow sticks represent dendron head groups. Colored spheres are adopted to represent the various hydrophobic regions of the micelles. A light gray field is used to represent water. DNA molecules are depicted as orange sticks. Reprinted with permission from Jones, S.P.; Gabrielson, N.P.; Wong, C.H.; Chow, H.F.; Pack, D.W.; Posocco, P.; Fermeglia, M.; Pricl, S.; Smith, D.K. *Hydrophobically modified dendrons: developing structure-activity relationships for DNA binding and gene transfection. Mol Pharm.*, 2011, 8(2), 416–429. Copyright {2012} American Chemical Society.

Most importantly, the experimentally verified CE_{50} values directly correlate with the surface charge density values σ_m estimated from the multiscale simulations, indicating that the micelles characterized by higher values of σ_m (i.e., Chol-G1-SP, C_{12} Lys-G1-SP, and D_2 Gly-G1-SP) are tighter DNA binders than their counterparts with lower σ_m values (i.e., C_{12} -G1-SP and D_1 Gly-G1-SP). Interestingly, comparing the best DNA binders, Chol-G1-SP, C_{12} Lys-G1-SP and D_2 Gly-G1-SP, the former compound assembles into micelles of much smaller diameter than the latter two. This is presumably due to the less sterically demanding nature of cholesterol leading to more effective packing within the micellar interior, compared with the branched hydrophobic units in the latter two dendrons, which will not be able to pack so efficiently. As such, even though the micelles formed by Chol-G1-SP contain fewer dendron units and have less total positive charge than the micelles formed by C_{12} Lys-G1-SP and D_2 Gly-G1-SP, their smaller size means that they have significantly higher surface charge density, and as such, they are therefore much more effective as DNA binders.

According to the classical laws of thermodynamics, the free energy of micellization ΔG_{mic} – i.e., the driving force that might eventually lead the amphiphilic molecules to spontaneously aggregate in water – can be expressed in the simple form $\Delta G_{mic} = -RT \ln K_m$, where K_m is the equilibrium constant between the aggregated and free forms of the given amphiphile in the aqueous environment. For conditions near or above the CMC, it can be shown that the above expression for ΔG_{mic} can be approximated to the form $\Delta G_{mic} = RT \ln(CMC)$. Accordingly, once either ΔG_{mic} or CMC is known, the other parameter can be easily estimated through this simple, fundamental relationship.

From an energetic standpoint, the change in Gibbs free energy of transfer of a single amphiphilic molecule from the monomeric state to a micelle of aggregation number N_{agg} , that is ΔG_{mic} , can be modeled as consisting of a hydrophobic part, $\Delta G_{mic,h}$, and an electrostatic part, $\Delta G_{mic,e}$, so that $\Delta G_{mic} = \Delta G_{mic,h} + \Delta G_{mic,e}$. The hydrophobic part stems primarily from the favorable energy of transfer of the hydrocarbon moieties from the aqueous phase to the micellar phase, and, secondarily, from the unfavorable residual interfacial contact of water with the apolar components within the micelles. The electrostatic part of ΔG_{mic} arises from the repulsion between the ionic head groups within the micellar shell.

Following the theory originally proposed by Tanford and subsequently modified by other authors, and using the information available from our multiscale simulations, we were able to calculate

the values of ΔG_{mic} and the corresponding CMCs for the five modified dendrons of Figure 12, as shown in Table 5. As it can be seen from this Table, ΔG_{mic} at room temperature has large, negative values, indicating that micellization is a spontaneous and highly favorable process for all amphiphilic dendrons, although ΔG_{mic} decreases on going from Chol-G1-SP to D_1 Gly-G1-SP. Since the head group architecture is the same in all amphiphiles, the main differential contribution to ΔG_{mic} must originate from the $\Delta G_{mic,h}$ term, which reflects differences in the size and structure of the hydrophobic component.

Table 5 – Predicted free energy of micellization ΔG_{mic} (kJ/mol) and critical micelle concentration CMC (μM) for the different modified dendrons of Figure 12. Reprinted with permission from Jones, S.P.; Gabrielson, N.P.; Wong, C.H.; Chow, H.F.; Pack, D.W.; Posocco, P.; Fermeglia, M.; Pricl, S.; Smith, D.K. *Hydrophobically modified dendrons: developing structure-activity relationships for DNA binding and gene transfection. Mol Pharm.*, **2011**, 8(2), 416–429. Copyright {2012} American Chemical Society.

Compounds	ΔG_{mic}	CMC
Chol-G1-SP	–87.56	0.021
C_{12} Lys-G1-SP	–80.42	0.089
D_2 Gly-G1-SP	–77.97	0.15
C_{12} -G1-SP	–55.92	12.5
D_1 Gly-G1-SP	–49.29	47.6

Typically, micellar aggregates have CMCs of the order of 10^{-3} – 10^{-5} M, while lower CMCs, even down to the nanomolar range can be found for amphiphiles that form either membranes or cylindrical aggregates. Recently, however, electron microscopy experiments performed on cholesterol-porphyrin micelles revealed that these amphiphiles could form virtually monodisperse spherical aggregates with a diameter of approximately 7 nm and a CMC value of 11 nM. Amphiphiles showing low CMCs tend to have relatively large hydrophobic segments, and this normally results in an assembly shape with a lower curvature. However, our series of modified dendrons combine a large hydrophobic portion with a very large head group, resulting in a roughly conical amphiphile. The size of the hydrophobic segment is responsible for the low CMCs, while the large size of the head group results in the spherical geometry of the assembly.

It is of particular interest to note that the predicted CMC values for C_{12} -G1-SP and D_1 Gly-G1-SP lie above the concentrations of the DNA binding assays (i.e. low μM concentrations) – as such, it is possible that the relatively poor DNA binding ability of these compounds reflects the fact that they

are not aggregated under the experimental conditions as a consequence of their relatively small hydrophobic segments. Although a word of caution is due about the fact that the calculated values of ΔG_{mic} and CMC are obtained using validated but simplified theoretical approaches, the trends exhibited by these parameters are in line with the experimental data. Indeed, we were able to carry out full experimental aggregation studies on a closely related set of hydrophobically modified dendrons, and for these systems, the *in silico* predictions of micelle diameters, charge densities and CMC values were closely mirrored by the experimental results, both in terms of trends and absolute values, thus strengthening not only the reliability of the entire computational procedure applied but, perhaps more importantly, validating its predictive capacity.

In concluding, Figure 15 graphically recaps the major finding of the study summarized and discussed above in terms of a graphical perspective of the qualitative relationship between the main properties of the self-assembled dendron systems investigated and their performance as gene delivery nanovectors.

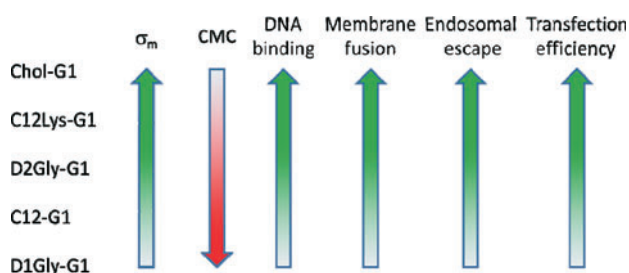


Fig. 15 – Qualitative SAR of the main properties of the self-assembled dendron systems and their performance as gene delivery nanovectors. The green color denotes a positive effect while the red color a negative one. The direction of the arrow head indicates an increase (upward direction) or a decrease (downward direction) of the relevant property/performance.

Conclusions

The extensive series of examples illustrated and discussed above – taken from our own experience in the field – emphasizes the role and potentiality of multiscale molecular modeling in the pre- and post-development of nanodevices for gene delivery. Accurate and reliable molecular modeling can be performed more easily than experiments. *In silico* evaluation can take into account the molecular specificity of the problem and dramatically reduce the time and cost required to formulate a new device and therapeutic intervention, and eventually translate it into the clinical setting. In nanomedicine, the need for accurate multiscale molecular modeling is even more pressing. Despite its

rapid growth and extraordinary potential, the field is still in its infancy, is highly interdisciplinary, and aims at solving problems of extraordinary and unprecedented complexity. With such a scenario, multiscale molecular modeling could afford a substantial contribution in dictating the success of nanomedicine and make the difference between several years of unfruitful research and the development of new, revolutionary therapeutic strategies readily available to the public.

ACKNOWLEDGMENTS

This wonderful experience in the multiscale molecular modeling of dendrimers and dendrons for gene therapy benefitted from a series of exciting and inspiring collaborations. The concrete chance for these collaborations originated under the framework of the Cost Action TD 0802 “Dendrimers in Biomedical Applications”, chaired by Prof. Barbara Klajnert, to which all authors are very much indebted. Financial support from the associated projects “DENANORNA” (International ERA-Net EUROMANOMED grant), “DDOS” (ESTECO grant), the HPC-Europa 2 Project (CINECA Supercomputing Center grant in the Eu 7th Framework Program), and “MONALISA” (Iscra supercomputing grant) is gratefully acknowledged. We also take the opportunity to thank our reviewers for their enthusiastic comments and helpful suggestions.

References

- Roco, M.C. *J. Nanoparticle Res.* **6** (2004) 1.
- See, for instance: a) Wang, M., Thanou, M. *Pharm. Res.* **62** (2010) 90; b) Mishra, B., Patel, B.B., Tiwari, S. *Nanomedicine: Nanotech. Biol. Med.* **6** (2010) 9; c) Sakamoto, J.H., van de Ven, A.L., Godin, B., Blanco, E., Serda, R.E., Grattoni, A., et al. *Pharmacol. Res.* **62** (2010) 57; d) de Martinprey, H., Vauthier, C., Malvy, C., Couvreur, P. *Eur. J. Pharm. Biopharm.* **71** (2009) 490; e) Christian, D.A., Cai, S., Bowen, D.M., Kim, Y., Pajeroski, D., Discher, D.E. *Eur. J. Pharm. Biopharm.* **71** (2009) 463; f) Singh, R., Lillard, J.W. *Exp. Mol. Pathol.* **86** (2009) 215; g) Ferrari, M. *Curr. Opin. Chem. Biol.* **9** (2005) 343; h) Ferrari, M. *Nat. Rev. Cancer* **5** (2005) 161.
- Ruenraroengsak, P., Cook, J.M., Florence, A.T. *J. Control. Release* **141** (2010) 265.
- For a very recent and by no means exhaustive list of reviews on these topics, see for instance: a) Watts, J.K., Corey, D.R. *J. Pathol.* **226** (2012) 365; b) Both, G., Alexander, I., Fletcher, S., Nicolson, T.J., Rasko, J.E., Wilton, S.D., Symonds, G. *Pathology* **43** (2011) 642; c) Gambari, R., Fabbri, E., Borgatti, M., Lampronti, I., Finotti, A., Brognara, E., Bianchi, N., Manicardi, A., Marchelli, R., Corradini, R. *Biochem. Pharmacol.* **82** (2011) 1416; d) Shukla, G.C., Haque, F., Tor, Y., Wilhelmsson, L.M., Toulmé, J.J., Isambert, H., Guo, P., Rossi, J.J., Tenenbaum, S.A., Shapiro B.A. *ACS Nano* **5** (2011) 3405 and references therein.

5. a) *Reischl, D., Zimmer, A.* Nanomedicine: Nanotech. Biol. Med. **5** (2009), 8; b) *Juliano, R., Alam, R., Dixit, V., Kang, H.* Nucl. Acid Res. **36** (2008), 4158; c) *Behr, J.P.* Acc. Chem. Res., Article ASAP, Publication Date (Web): February 6, 2012, DOI: 10.1021/ar200213g; d) *Mintzer, M.A., Simanek, E.E.*, Chem. Rev. **109** (2009), 259; e) *Jeong, J.H., Kim, S.W., Park, T.G.* Progr. Polym. Sci. **32** (2007) 1239.
6. *Posocco, P., Fermeglia, M., Pricl, S.* J. Mater. Chem. **20** (2010) 7742.
7. *Tomalia, D.A.* Progr. Poly. Sci. **30** (2005) 294.
8. *Tomalia, D.A., Naylor, A.M., Goddard, W.A.* III. Angew. Chem. Int. Ed. Engl. **29** (1990) 138.
9. *Svenson, S.* Eur. J. Pharm. Biopharm. **71** (2009) 445.
10. *Liu, M., Frechet, J.M.*, Pharm. Sci. Technol. Today **2** (1999) 393.
11. a) *Cheng, Y., Zhao, L., Li, Y., Xu, T.* Chem. Soc. Rev. **40** (2011) 2673; b) *Mintzer M.A., Grinstaff M.W.* Chem. Soc. Rev. **40** (2011) 173; c) *Medina, S.H., El-Sayed, M.E.H.* Chem. Rev. **109** (2009) 3141; d) *Tekade R.K., Kumar, P.V., Jain, N.K.* Chem. Rev. **109** (2009) 49–87; e) *Rolland, O., Turrin, C.O., Caminade, A.M., Majoral, J.P.* New J. Chem. **33**, (2009) 1809.
12. *Hoogerbrugge, P.J., Koelman, J.M.V.A.* Europhys. Lett. **19** (1992), 155; b) *Español, P., Warren, P.B.* Europhys. Lett. **30** (1995) 191; c) *Groot, R.D., Warren, P.B.* J. Chem. Phys. **107** (1997) 4423.
13. See, for instance: a) *Posocco, P., Laurini, E., Dal Col, V., Marson, D., Karatasos, K., Fermeglia, M., Pricl, S.* Curr Med. Chem. accepted, in press (2012); b) *Toth, R., Santese, F., Pereira, S.P., Nieto, D.R., Pricl, S., Fermeglia, M., Posocco, P.* J. Mater. Chem., J. Mater. Chem. **20** (2010) 10511; c) *Scocchi, G., Posocco, P., Handgraaf, J.-W., Fraaije, J.G., Fermeglia, M., Pricl, S.* Chem. Eur. J. **15** (2009) 7586; d) *Toth, R., Voorn, D.-J., Handgraaf, J.-W., Fraaije, J.G.E.M., Fermeglia, M., Pricl, S., Posocco, P.* Macromolecules **42** (2009) 8260; e) *Fermeglia, M., Pricl, S.* Computers & Chem. Eng. **33** (2009) 1701 and references therein.
14. a) *Karatasos, K., Posocco, P., Laurini, E., Pricl, S.* Macromol Biosci. **12** (2012) 225; b) *Liu, X., Liu, C., Laurini, E., Posocco, P., Pricl, S., Qu, F., Rocchi, P., Peng, L.* Mol. Pharm. **9** (2012) 470; c) *Liu, X.X., Wu, J., Yamine, M., Zhou, J., Posocco, P., Viel, S., Liu, C., Ziarelli, F., Fermeglia, M., Pricl, S., Victorero, G., Nguyen, C., Erbacher, P., Behr, J.P., Peng, L.* Bioconjug. Chem. **22** (2011) 2461; d) *Pavan, G.M., Posocco, P., Tagliabue, A., Maly, M., Malek, A., Danani, A., Ragg, E., Catapano, C.V., Pricl, S.* Chemistry Eur. J. **16** (2010) 7781; e) *Posocco, P., Ferrone, M., Fermeglia, M., Pricl, S.* Macromolecules **40** (2007) 2257; f) *Metullio, L., Ferrone, M., Coslanich, A., Fuchs, S., Fermeglia, M., Paneni, M.S., Pricl, S.* Biomacromolecules **5** (2004) 1371; g) *Pricl, S., Fermeglia, M., Ferrone, M., Asquini, A.* Carbon **41** (2003) 41 2269; h) *Fermeglia, M., Ferrone, M., Pricl, S.* Bioorg. Med. Chem. **10** (2002) 2471.
15. a) *Prosa, T. J., Bauer, B. J., Amis, E. J., Tomalia, D. A., Scherrenberg, R. J.* Polym. Sci. B: Polym. Phys. **35** (1997) 2913; b) *Rathgeber, S., Monkenbusch, M., Kreitschmann, M., Urban, V., Brulet, V.* J. Chem. Phys. **117** (2002) 4047.
16. a) *Maiti, P. K., Cagin, T., Lin, S. T., Goddard W. A.* III Macromolecules **38** (2005) 979; b) *Maiti, P. K., Messina R.* Macromolecules **41** (2008) 5002.
17. *Srinivasan, J., Cheatham, T. E., Cieplak, P., Kollman, P. A., Case, D. A.*, J. Am. Chem. Soc. **120** (1998) 9401.
18. See, for instance: a) *Gomez-Casado, A., Dam, H.H., Yilmaz, M.D., Florea, S., Jonkheijm, P., Huskens, J.* J. Am. Chem. Soc. **133** (2011) 10849; b) *Kane, R.S.* Langmuir **26** (2010) 8636; c) *Badjic, J.D., Nelson, A., Cantrill, S.J., Turnbull, W.B., Stoddard, J.F.* Acc. Chem. Res. **38** (2005) 723; d) *Huskens, J., Mulder, A., Auletta, T., Nijhuis, C.A., Ludden, M.J.W., Reinhoudt, D.N.* J. Am. Chem. Soc. **126** (2004) 6784; e) *Christensen, T., Gooden, D.M., Kung, J.E., Toone, E.J.* J. Am. Chem. Soc., **125** (2003) 7357, f) *Kitov, P.I., Bundle, D.R.* J. Am. Chem. Soc. **125** (2003) 16271.
19. *Rosen, B.M., Wilson, C.J., Wilson, D.A., Peterca, M., Imam, M.R., Percec, V.* Chem. Rev. **109** (2009) 6275.
20. *Smith, D.K., Hirst, A.R., Love, C.S., Hardy, J.G., Brignell, S.V., Huang, B.* Prog. Polym. Sci. **30** (2005) 220.
21. a) *Hamley, J.W.* Angew. Chem. Int. Ed. **42** (2003) 1692; b) *Whitesides, G.M., Grzybowski, B.* Science **295** (2002) 2418.
22. a) *Steed, J.W., Atwood, J.L.* Supramolecular Chemistry. Wiley & Sons: Chichester, 2000; b) *Beer, P.D., Gale, P.A., Smith, D.K.* Supramolecular Chemistry. Oxford University Press: Oxford, 1999.
23. a) *Jones, S.P., Gabrielson, N.P., Wong, C.H., Chow, H.F., Pack, D.W., Posocco, P., Fermeglia, M., Pricl, S., Smith, D.K.* Mol Pharm. **8** (2011) 416; b) *Barnard, A., Posocco, P., Pricl, S., Calderon, M., Haag, R., Hwang, M.E., Shum, V.W., Pack, D.W., Smith, D.K.* J. Am. Chem. Soc. **133** (2011) 20288; c) *Jones, S.P., Pavan, G.M., Danani, A., Pricl, S., Smith, D.K.* Chem. Eur. J. **16** (2010) 4519; d) *Posocco, P., Pricl, S., Jones, S.P., Barnard, A., Smith, D.K.* Chem. Sci. **1** (2010) 393; e) *Pavan, G.M., Danani, A., Pricl, S., Smith, D.K.* J. Am. Chem. Soc. **131** (2009) 131 9686.
24. (a) *Israelachvili, J.N., Mitchell, D.J., Ninham, B.W.* Biochim. Biophys. Acta, Biomembr. **470** (1977) 185; b) *Israelachvili, J.N., Mitchell, D.J., Ninham, B.W.* J. Chem. Soc., Faraday Trans. II **72** (1976) 1525.
25. *Abdelhady, H.G., Allen, S., Davies, M.C., Roberts, C.J., Tendler, S.J.B., Williams, P.M.* Nucleic Acid Res. **31** (2003) 4001.
26. a) *Dorigo, B., Schalch, T., Kulangara, A., Duda, S., Schroeder, R., Richmond, T.J.* Science **306** (2004), 1571; b) *Olins, A.L., Olins, D.E.* Science **183** (1974) 330.
27. *Tanford, C.* The hydrophobic effect: formation of micelles and biological membranes, 2nd ed. Krieger Publishing Co., Malabar, FL, 1991.
28. a) *Patrickios, C.S.* J. Phys. Chem. **99** (1995) 17437; (b) *Nagarajan, R.* Langmuir **18** (2002) 31.
29. *Tomas, S., Milanese, L.* J. Am. Chem. Soc. **131** (2009) 6618.